Technical Report | 353

Field Emission in Vacuum Voltage Breakdown

G. E. Vibrans

8 May 1964

Lincoln Laboratory

MASSACHUSETTS INSTITUTE OF TECHNOLOGY

Lexington, Massachusetts

MASSACHUSETTS INSTITUTE OF TECHNOLOGY

LINCOLN LABORATORY

FIELD EMISSION IN VACUUM VOLTAGE BREAKDOWN

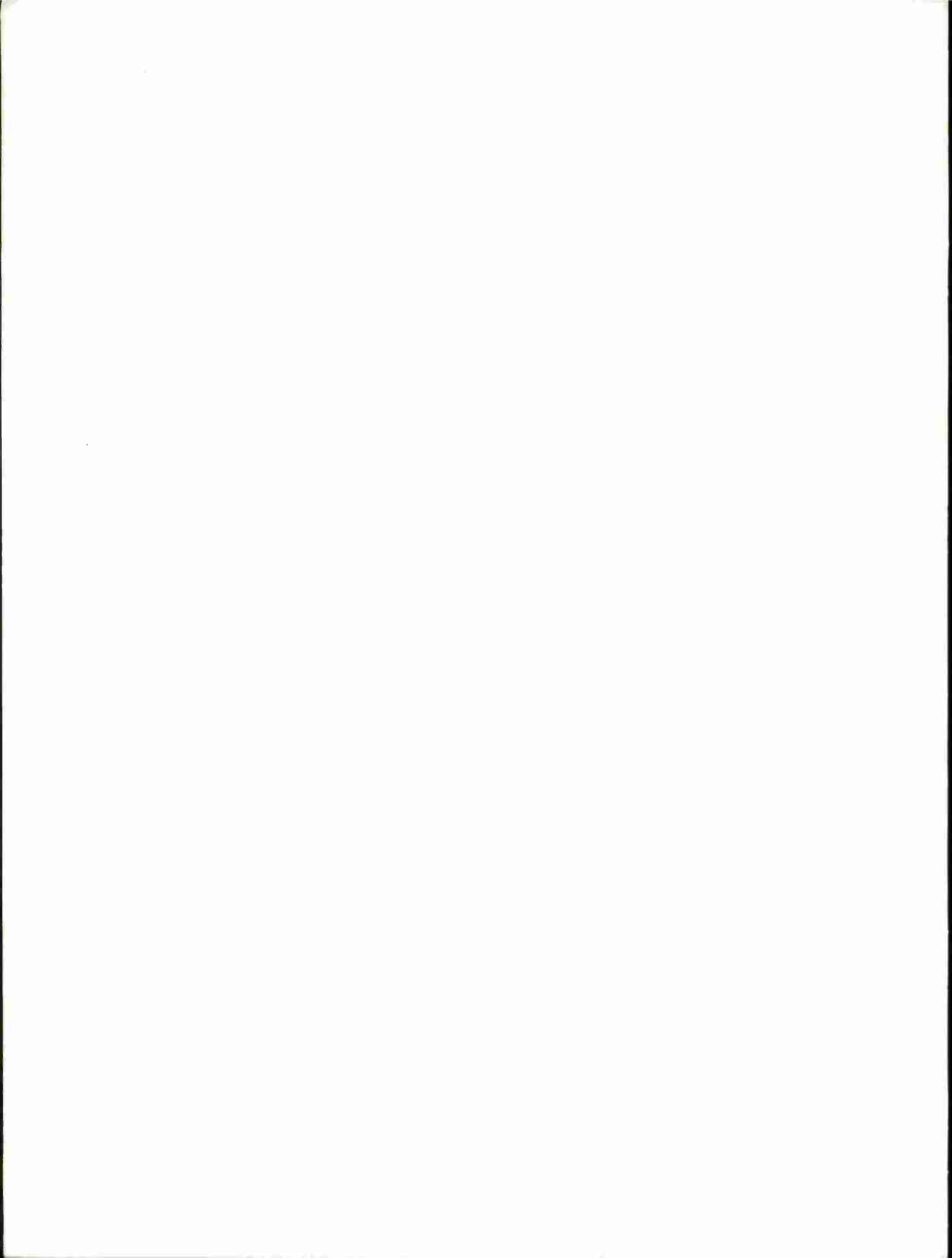*G. E. VIBRANS*

Group 43

TECHNICAL REPORT 353

8 MAY 1964

LEXINGTON   MASSACHUSETTS

ABSTRACT

Field intensification and emitting area are determined for a spheroid and a whisker-shaped protrusion. The effects of an inhomogeneous field around a protrusion on the transmission coefficient for field emission are computed, and examples are given. The resistive heating of an emitter is analyzed for a case in which both the resistivity and the emission are temperature dependent. An instability is pointed out, and the external resistance which stabilizes the emission of a whisker is given. The spreading of the emitted beam due to field distortion at the protrusion and to space-charge repulsion is computed separately and given in general form. It is concluded that the beam spreads faster than previous hypotheses assume. The formation of small craters at the anode by single electron beams is questioned.

TABLE OF CONTENTS

FIELD EMISSION IN VACUUM VOLTAGE BREAKDOWN

I.   INTRODUCTION

Many authors have interpreted the prebreakdown currents in a vacuum as field emission coming from small sharp protrusions which intensify the field locally.   Surface contamination, insulating patches on the electrode, loose particles, or avalanches of particle interchange are also suspected of causing breakdown.   However, the recent works of Little[1] and of Tomaschke,[2] as well as many earlier reports, leave no doubt that for clean conditions the prebreakdown current due to field emission is somehow the cause of the breakdown.

The emitting protrùsions are usually compared with spheroids because a closed mathematical expression exists for the field.   We believe that a more complete mathematical analysis of prebreakdown currents is possible, but that the spheroid is not the best model for a protrusion.   The spheroid is neither a typical model for the shapes which have been observed nor is it the most efficient emitter.   In Secs. II and III we derive the field intensification β and emitting area A for an optimum emitter as well as for a spheroid.   This gives us the minimum height for any protrusion with known β and A.   Another limit on the radius of curvature, and hence on the size of any emitter, follows from the computation of field emission in an inhomogeneous field (Sec. IV).   The computation of resistive heating and of beam spreading in Secs. V and VI gives arguments for and against several breakdown hypotheses.

A.   Field Emission and Breakdown

For a recent review of the hypotheses which try to explain vacuum voltage breakdown, see Hawley,[3] Bettenhausen,[4] and Little.[5]   One hypothesis is that the field emission heats the anode and evaporates it locally, thus initiating a gas discharge.[6]   The final temperature in the middle of a bombarded circle on the anode surface may be expressed as follows:

$$T_a = \frac{i_a UQd}{2\lambda}$$
(1)

This is the limit for $t = \infty$ of the general equation given in the literature.[7]   The product $i_a UQ$ is the bombarding power density in calories per square centimeter.   We can write instead

$$T_a = \frac{UQ \sqrt{i_a I}}{\lambda \sqrt{\pi}}$$
(2)

where I is the total bombarding current and i_a is the bombarding current density.   Equation (2) shows that the product of total current and current density determines the anode temperature.

The current density at the anode can be computed from the emission density[8] which, together with the total current, is determined by cathodic processes. We see that we need to consider the total emission and the emission density as equally important for breakdown, i.e., if Eq. (2) applies.

Another hypothesis is that a microscopic protrusion at the cathode is heated by the field emission current, so that it evaporates and ignites the arc. This was first proposed by Ahearn[9] in 1936 and has been supported by his experimental results. Ahearn used cylindrical gaps in sealed tubes with thin tungsten-wire cathodes – mostly thoriated. Tuczek[10] observed the emission of protrusions in large gaps under high voltages (up to 600 kv) and different pulse lengths. He interpreted some of the photographs as protrusions in various stages of temperature-field emission. Schwabe[11] also gave some support for this hypothesis, and showed that there is a prebreakdown material transfer from cathode to anode as well as the larger transfer from anode to cathode. Dyke[12] has proven that the temperature rise of an emitting protrusion ignites an arc under certain conditions. Alpert[13] recently showed that this cathodic process may also explain the results of Boyle.[14] Alpert remarked, however, that an analysis of what really happens when the emitter ignites the arc is still missing.

The emission density depends on the local field, i.e., on the shape of the protrusion but not on its absolute size (in a parallel field). The radius of the emitting area is proportional to the absolute dimensions of the emitter; the current is therefore proportional to the square of the size for any given shape.

For a detailed investigation of the field emission, we must choose a suitable family of shapes for a protrusion, which allows us to reach any field intensification we want. Of course, any "sharp" corner will give a very high field intensification. But the field strength which actually occurs is limited by the mechanical strength of the cathode material. Obviously, we must always consider a protrusion with a finite radius of curvature – however small that may be.

II. FIELD INTENSIFICATIONS

A. Sphere

For any given height and given emitting area, a sphere on the tip of an infinitesimally thin wire should give the highest possible field intensification. We can approximate this field with a suitably charged sphere in a homogeneous field. The potential distribution is

$$\Phi = E_\infty(z + h - R) - \frac{E_\infty R^3 z}{(x^2 + y^2 + z^2)^{3/2}} - \frac{q}{4\pi\epsilon_o \sqrt{x^2 + y^2 + z^2}} \tag{3}$$

as shown schematically in Fig. 1. The surface which has the same potential as the sphere is not exactly a plane. We could eliminate the distortion in the plane by adding the mirror image of the sphere, but this would then distort the sphere, making necessary further mirror images of a higher order. We neglect the distortion of the electrode surface ($\Phi = 0$) which is permissible as long as h is several times larger than R.*

---

* The height of the distortion δ of the electrode plane approximates the radius R of the sphere:

$$\delta \approx \frac{\Phi(z = -h + R)}{E_\infty} = R \left\{ 1 - \frac{1}{[(h/R) - 1]^2} \right\} .$$

Fig. 1. Potential distribution of a sphere on an infinitesimally thin wire.
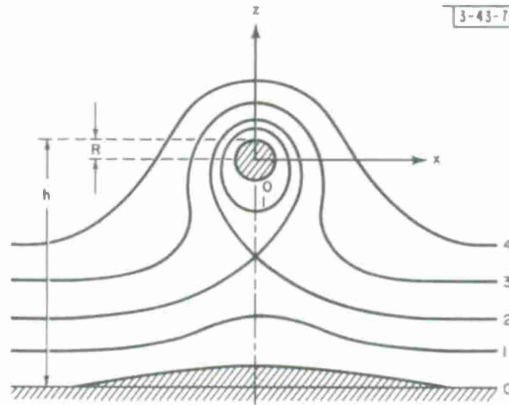
The condition

$$\Phi = 0 \quad \text{at} \quad \sqrt{x^2 + y^2 + z^2} = R \tag{4}$$

determines the charge of the sphere

$$q = E_\infty (h - R)\, 4\pi\epsilon_0 R \quad . \tag{5}$$

From Eqs. (3) and (5), the field intensification at the tip ($x = y = 0$, $z - R$) is

$$E_\infty \beta = \frac{\partial \Phi}{\partial z} = E_\infty \left(3 + \frac{h - R}{R}\right) \tag{6}$$

$$\beta = 2 + \frac{h}{R} \quad . \tag{7}$$

The field intensification is dependent on the ratio of dimensions only and not on absolute size.

B. Rounded Wire (Whisker)

A less idealized shape of a protrusion is a wire with a spherical cap. No closed expression is known for such a field, but we have computed it numerically by distributing a number (e.g., 20) of charges along the line from $z = -h + R$ to $z = 0$ (cf. Fig. 1) and adding the mirror charges along $z = -2h + 2R$ to $z = -h + R$. For a number of points (e.g., 40) along the contour of the protrusion, the induced potential is computed, and the charges are determined so that the sum of the squared potentials at the contour points becomes a minimum. This amounts to the inversion of a 20 by 20 matrix. A standard routine of the 7090 computer was used. To check the validity, we computed the potential half way between the contour points.

The shape of such a body is shown in Fig. 2, with the deviation from the ideal much exaggerated. The deviations are less than 0.07 percent at the cap.

An example with $h = 10$ and $R = 1$ is given in the Appendix. The field intensification is $\beta = 11.81$, compared with a sphere for which Eq. (7) gives $\beta = 12$. We see from the table in the Appendix that the field on the rounded whisker is very similar to that of a sphere. Therefore, we are justified in using the mathematically simpler sphere as a model for a very pointed and strongly emitting protrusion.

C. Spheroid

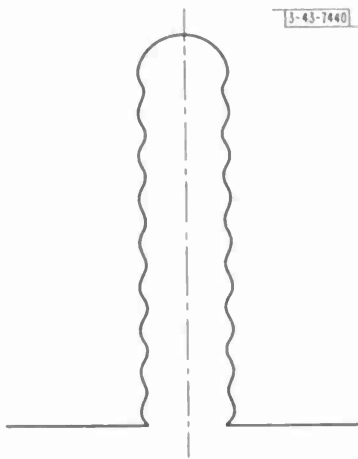Still another model of a protrusion is a spheroid which is often used as a reference.

3

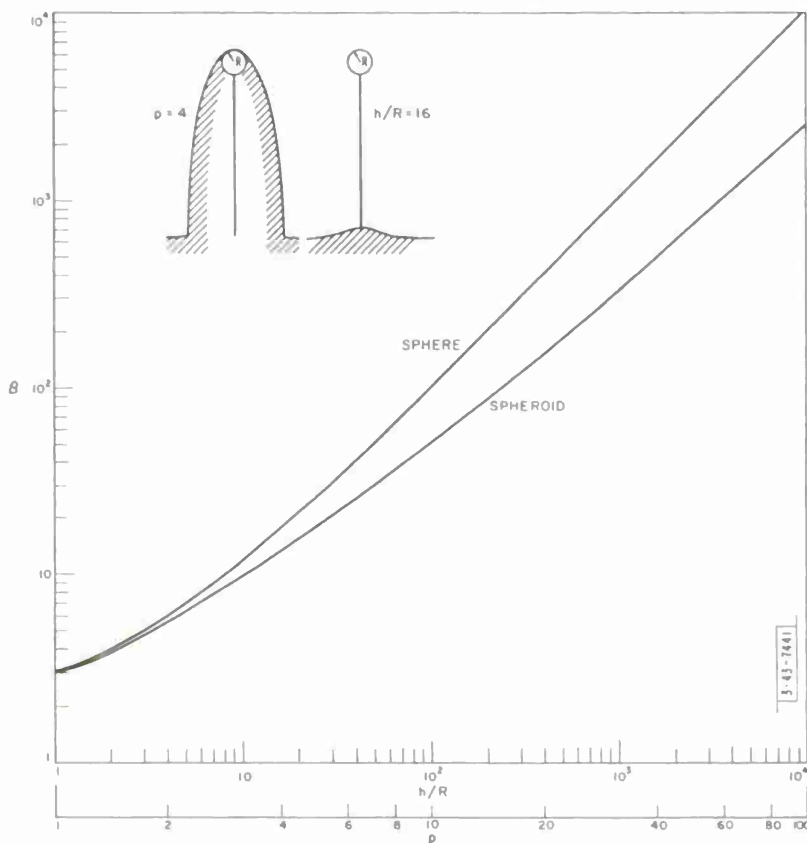Fig. 2. Shape of a protrusion (wire with a spherical cap).

Fig. 3. Field intensification at apex of both a sphere and spheroid $\beta = E_{max}/E_\infty$ vs $p = b/a$ and h/R.

4

The equatorial plane of the spheroid is an equipotential plane and represents the electrode surface. The field intensification at the tip of the spheroid is given by the expression:

$$\beta = \frac{E}{E_\infty} = \frac{1}{N} \quad , \quad N = \frac{1}{p^2 - 1} \left[\frac{p}{\sqrt{p^2 - 1}} \ln \left(p + \sqrt{p^2 - 1} \right) - 1 \right] \quad . \tag{8}$$

The number N is known as the demagnetizing or depolarizing factor; $p = b/a$ is the ratio of axes (b = major axis). Here again the field intensification is independent of the absolute size of the spheroid.

To make a comparison, we have plotted (Fig. 3) the field intensification for both a sphere and a spheroid vs the height normalized with the radius of curvature. The radius of curvature at the apex of the spheroid is $R = a^2/b$. The ratio of the axis for the spheroid $p = b/a$ is shown as a second scale on the abscissa.

III. EMITTING AREA OF A SPHEROID AND SPHERE

Now we can determine the total emitted current or the emitting area. First we need to know how the field strength varies around the tip. The field perpendicular to the surface of a dielectric spheroid is $E_\perp = E_{2\epsilon} \cos \Theta$ (Fig. 4). The conducting spheroid is characterized by $\epsilon \to \infty$, $E_2 \to 0$, while $E_{2\epsilon}$ remains finite and independent of Θ. With Eq. (8), the field on the surface of the conducting spheroid becomes

$$E_\perp = \frac{1}{N} E_\infty \cos \Theta = \frac{1}{N} E_\infty \frac{1}{\sqrt{1 + \frac{x^2}{a^2 - x^2} \frac{b^2}{a^2}}} \tag{9}$$

for the sphere:

$$E_\perp = 3E_\infty \cos \Theta + \frac{h - R}{R} E_\infty = 3E_\infty \cos \Theta + (\beta - 3) E_\infty \tag{10}$$

where Θ is the angle between the surface normal and the axis of the protrusion. The relative field distribution vs the normalized lateral distance x/R is plotted in Fig. 5. We see that the emitting area of the sphere must be larger than that of the spheroid whose field decreases rapidly with the distance from the axis. We see also that the curves for different spheroids are very close together for $(h/R) \geqslant 25$, and that the first 20 percent of the decrease of the field is practically the same for all spheroids with $(h/R) \geqslant 25$. This is the only area of interest for us since a decrease of the field by 20 percent decreases the current density by orders of magnitude, according to the Fowler-Nordheim equation. The coincidence of the curves in Fig. 3 allows us to normalize the emitting area of a spheroid so that it only depends upon the intensified field at the tip [as long as $(h/R) \geqslant 25$].

The ring-shaped surface element where a certain field applies has the area (see Fig. 4)

$$dA = 2\pi x \frac{dx}{\cos \Theta} \quad . \tag{11}$$

The element of current from this area is

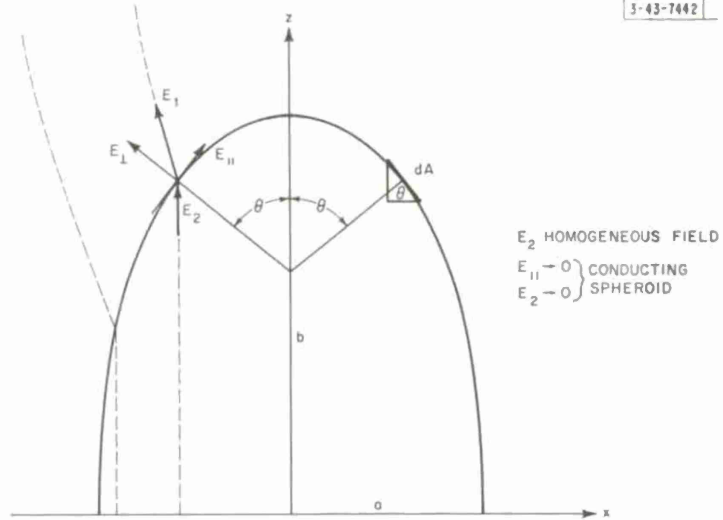$$dI = i_{em}(E) \cdot 2\pi x \cdot \frac{dx}{\cos \Theta} \quad . \tag{12}$$

5

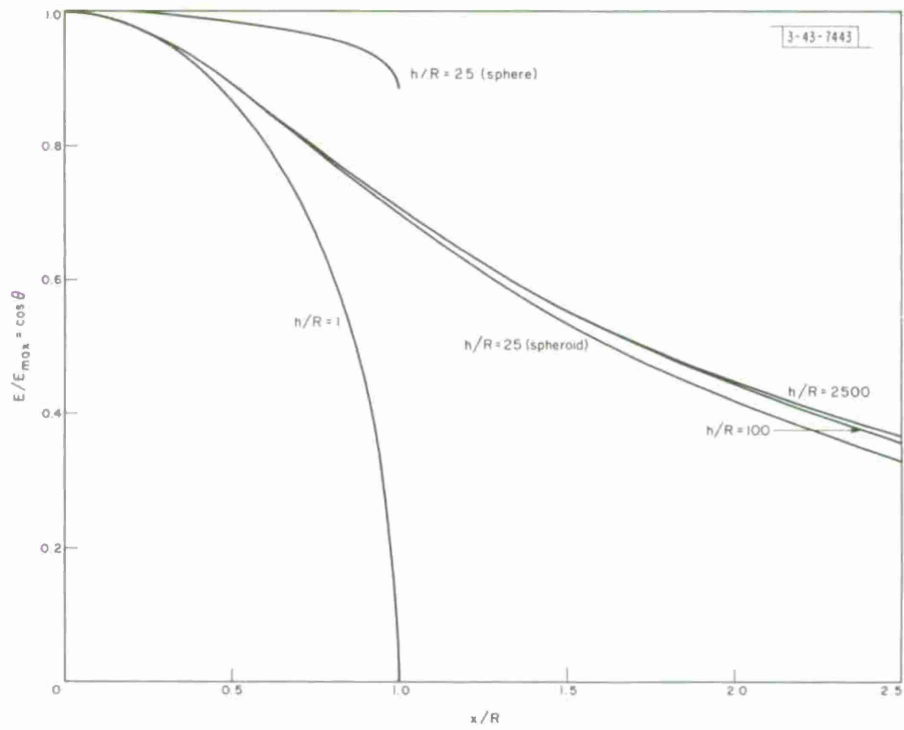Fig. 4. Geometry of the spheroid.

Fig. 5. Relative field strength $\cos \theta = E/E_{max}$ vs distance/radius of curvature x/R for both a sphere and spheroid.

6

The Fowler–Nordheim equation determines $i_{em}(E)$. Values given by Dyke[15] are used to plot Fig. 6. A work function of $\varphi = 4.5$ ev (e.g., clean copper electrodes) is always used.

We can integrate Eq. (12) numerically if we take $E(x)$ and $\cos\Theta$ from Eq. (9) and $i(E)$ from Fig. 6. The result is plotted in Fig. 7 as the normalized radius of a mean emitting area vs the field at the apex. The mean emitting area is defined by

$$I = \pi \bar{x}^2 i_{max} \tag{13}$$

where i_{max} is the emission density at the apex.

For the sphere, we can replace $(1/\cos\Theta)\, x\, dx$ by $R\sin\Theta\, d\Theta$ and the total current becomes

$$I = \int_0^{90^\circ} i(\Theta)\, 2\pi R^2 \sin\Theta\, d\Theta \quad . \tag{14}$$

For the field emission, we use the approximation

$$i = i_{ref}\, e^{nE} \tag{15}$$

where n and i_{ref} are constants which we must choose to fit the range over which Eq. (15) is intended to be valid. We insert Eqs. (10) and (15) into Eq. (14).

$$I = -2\pi R^2 i_{ref}\, e^{n(\beta-3)E_\infty} \int_1^0 e^{3n\cos\Theta E_\infty}\, d\cos\Theta$$

$$= 2\pi R^2 i_{ref}\, e^{n(\beta-3)E_\infty}\, \frac{e^{3nE_\infty} - 1}{3nE_\infty} \quad . \tag{16}$$

We introduce the surface of the emitting semisphere:

$$A_{sph} = 2\pi R^2 \tag{17}$$

and the maximum current density at the top of the protrusion

$$i_{max} = i_{ref}\, e^{nE_\infty\beta} \tag{18}$$

and write

$$I = A i_{max}\, \frac{1 - e^{-3nE_\infty}}{3nE_\infty} \quad . \tag{19}$$

The quantity n is a constant for each evaluation of the integral in Eq. (16) because the approximation covers two orders of magnitude of the current density. In Eq. (19), however, n is still a function of $E_{max} = E_\infty\beta$. Suitable values of n vs E_{max} are plotted in Fig. 8. They are determined so that Eq. (15) represents the chord of $\log i$ vs E between E_{max} and $E_{max} - 10^7$. Figure 9 gives

$$3nE_\infty \quad \text{vs} \quad \beta E_\infty$$

$$3nE_\infty \quad \text{vs} \quad \frac{1}{3nE_\infty}\left(1 - e^{-3nE_\infty}\right) \quad .$$

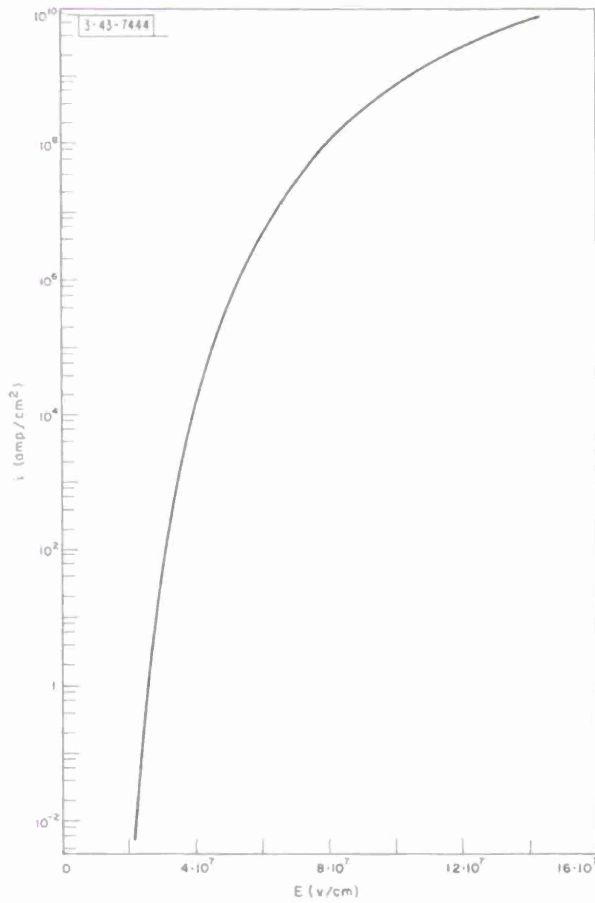Fig. 6. Field emission density i vs field strength E for a work function of $\phi = 4.5$ ev (Ref. 15).
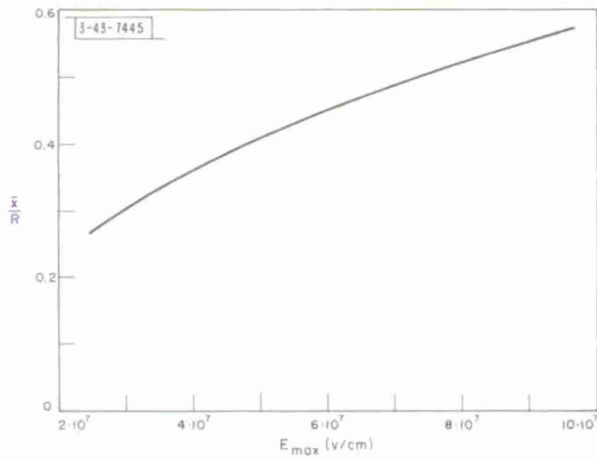

Fig. 7. Radius of mean emitting area/radius of curvature $\bar{x}/R$ vs the intensified field strength at apex of spheroid E_{max} for a work function of $\phi = 4.5$ ev.
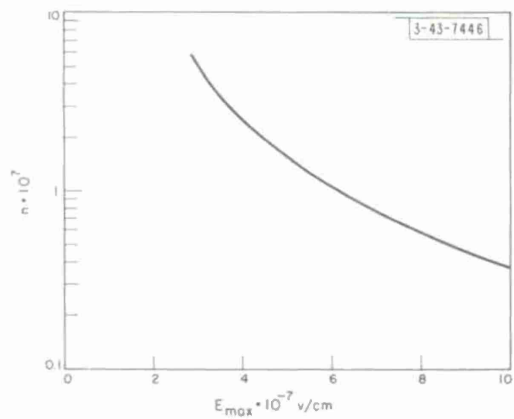

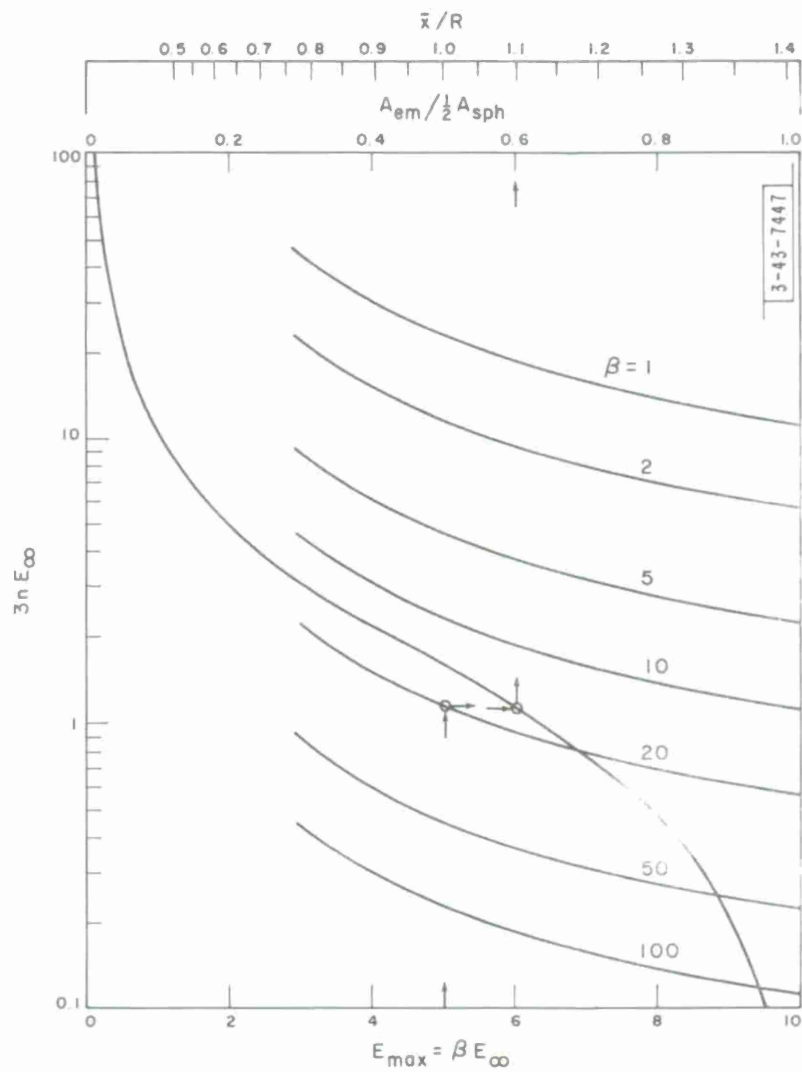Fig. 8. $n \cdot 10^7$ vs $E_{max} \cdot 10^{-7}$ v/cm.

Fig. 9. Determination of radius $\bar{x}$ of mean emitting area for a whisker-shaped protrusion.

This diagram allows us to determine the relative emitting area

$$\frac{A_{em}}{A_{sph}} = \frac{I}{I_{max}} \quad .$$

For comparison with Fig. 7, $\bar{x}/R$ can be read with a second scale. The application of the diagram is shown in Fig. 9 for an example where $E_\infty = 2.5 \cdot 10^6$ and $\beta = 20$ are given; and $E_{max} = 5.10^7$, $A_{em}/A_{sph} = 0.6$, and $\bar{x}/R = 1.1$ are found.

IV. FIELD EMISSION IN AN INHOMOGENEOUS FIELD

As Lewis first pointed out,[16] the field emission is affected by the inhomogeneity of the field because the field intensity may drop appreciably within the length of the potential barrier, thus modifying the tunnel effect. We compute the transmission coefficient by looking at one electron which leaves the apex of our spherical protrusion. The mathematical solution of the wave mechanical problem is given, e.g., in the Encyclopedia of Physics,[17] and we will only show where our analysis deviates from the standard solution.

The transmission coefficient D is given as

$$-\ln D = \int_{z_1}^{z_2} \sqrt{\frac{8m}{\hbar^2} \left[V(z) - W \right]} \, dz \tag{20}$$

where V is the potential energy of the electron.

The potential field in which the electron moves is represented by Eqs. (3) and (5) ($x = y = 0$), but we must add the potential of the mirror image (at $z_m = R^2/z$) of the electron

$$\Phi_m = -\frac{e}{4\pi\epsilon_o} \frac{R}{2(z^2 - R^2)} \quad . \tag{21}$$

We introduce

$$\xi = \frac{z - R}{R} \tag{22}$$

and insert Eqs. (3), (5), (7), and (21) into Eq. (20). Thus, the transmission coefficient becomes:

$$-\ln D = \int_{\xi_1}^{\xi_2} \sqrt{\frac{8me}{(h/2\pi)^2} \left(-E_\infty R\xi \, \frac{\beta(1 + \xi) + \xi^2}{(1 + \xi)^2} - \frac{e}{8\pi\epsilon_o R(2\xi + \xi^2)} + \frac{|W|}{e} \right)} \, R d\xi \tag{23}$$

where ξ_1 and ξ_2 are the values for which the radicand is zero. With Eq. (23), we compute the transmission coefficient numerically (Simpson's Rule) for given sets:

Radius of curvature of protrusion	R (cm)
Field intensification of protrusion	β
Homogeneous field away from protrusion	E_∞ (v/cm)
Work function	$\varphi = \dfrac{|W|}{e}$ (v)

In order to integrate over the product of supply function and transmission coefficient, we need D as a function of W or at least the derivative dD/dW. Instead of coding a second function, it is advantageous to compute D for two nearly equal values W_1 and W_2, and to approximate D(W) by the linear expression:

$$\ln D(W) = \ln D(W_1) + \frac{\ln D(W_2) - \ln D(W_1)}{W_2 - W_1} \, (W - W_1) \qquad . \tag{24}$$

This equation corresponds to Eq. (5.10) of Ref. 17. Now we can integrate in order to find the number of emitted electrons.

$$\frac{j}{e} = \int_{W=0}^{\varphi} \frac{4\pi m}{h^3} \, e \cdot \exp\left[\frac{\ln D_2 - \ln D_1}{W_2 - W_1} \, (W - W_1) + \ln D_1 \right] \cdot (\varphi - W) \, dW$$

$$= \frac{4\pi m}{h^3} \, D(\varphi) \, e \left(\frac{W_2 - W_1}{\ln D_2 - \ln D_1} \right)^2 \tag{25}$$

where e is the charge of the electron. The results of numerical computation for two work functions (2 and 4.5 ev) and several radii of curvature vs the intensified field are plotted in Fig. 10. The field intensification was assumed to be $\beta = 100$. As Lewis[16] has already explained, only the emission of very small protrusions (radius of the order of 10 Å) is affected. We see also that the emission lags mainly for smaller currents so that the current rises more abruptly with voltage.

Figure 10 is computed for a spherical protrusion, but it represents an approximation for other protrusions whose radii of curvature and field gradient are similar. For a spheroid, the field along the axis is given by Lewis[18] [watch the misprint: in Eq. (5) the last term must be raised to the minus first power] from which we derive the gradient at the tip: $d\beta/dz \approx -2\beta/R$. [We have assumed $(a^2/b^2) \ll 1$.] We find a similar expression for the gradient in front of the sphere if we differentiate Eq. (3) twice: $d\beta/dz = -2\beta/R$.
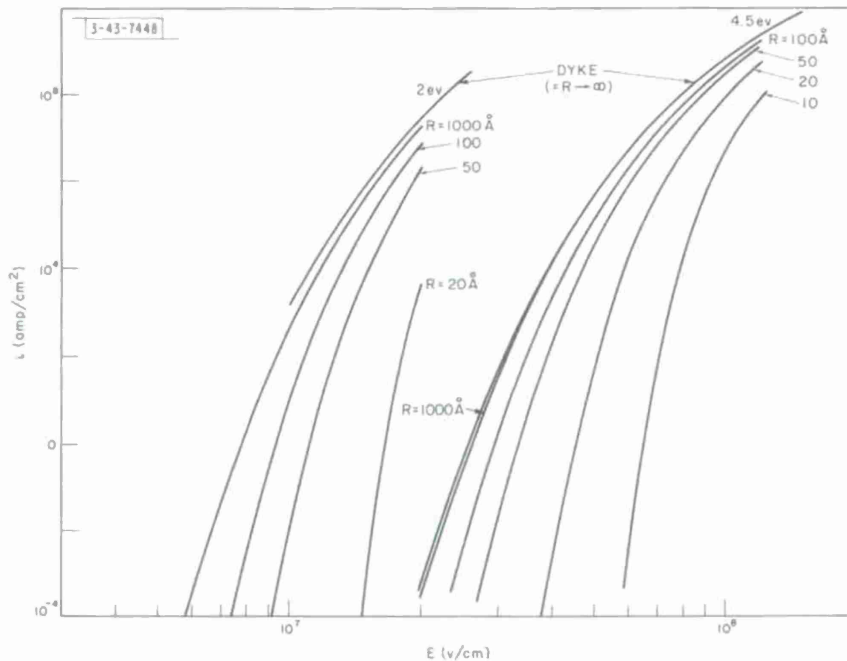

Fig. 10. Field emission current density vs local field strength for protrusions with field intensification $\beta = 100$, work functions of $\phi = 2$ and 4.5 ev, and several radii of curvature R. .

By looking at Figs. 7 and 9, we can say that Fig. 10 applies to spheroids with $\beta = 100$ if we assume that R is about twice the radius of the emitting area.

Let us append a proof that the field gradient at the tip of any protrusion essentially depends on R and β, so that Fig. 10 is generally valid.

The potential around the tip is represented by

$$\Phi = Ez + E' \frac{z^2}{2} + A(x^2 + y^2)$$

where x, y, z are Cartesian coordinates counting from the tip. The third and higher powers of distance from the tip are neglected, and the rotational equipotential surface $\Phi = 0$ with a maximum at $x = y = z = 0$ has been taken into account. The contour of the protrusion in the plane $y = 0$ is given by

$$Ez + E' \frac{z^2}{2} + Ax^2 = 0 \quad .$$

The radius of curvature at the tip is

$$R = \left\{ \frac{[1 + (dz/dx)^2]^{3/2}}{d^2z/dx^2} \right\}_{x=0} = -\frac{E}{2A} \quad .$$

With this and Laplace's equation $\Delta\Phi = 0$, we establish the relationship:

$$E' = \frac{\partial^2 \Phi}{\partial z^2} = 2 \frac{E}{R} \quad \text{Q.E.D.}$$

V. RESISTIVE HEATING OF THE PROTRUSION

A. Temperature of the Emitting Protrusion

The steady-state temperature of an emitting spheroid can be found in closed form. We assume the equatorial plane is held at a constant temperature. The heat conduction equation for steady state is

$$\frac{dT}{dz} = \frac{q}{\pi x^2 \lambda} \tag{26}$$

where q is the flow of heat generated between the heights z and z_1 (Fig. 11). From z_1 on, the emission becomes important, the current is no longer confined to the spheroid, and we neglect the heat produced between $z = z_1$ and $z = b$. This avoids formal difficulties with infinite current density at the apex. The heat generated by a current I is

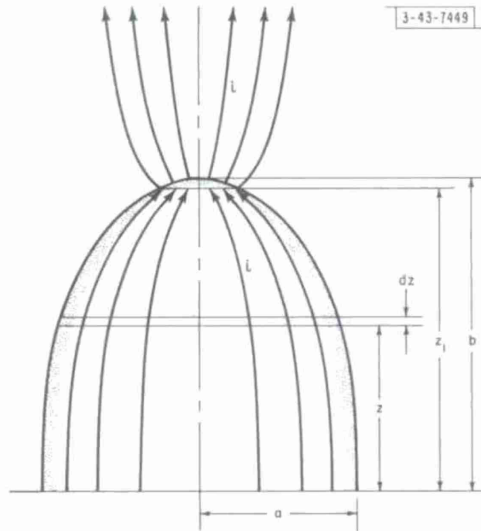$$q = \int_z^{z_1} \frac{I^2 Q}{\pi x^2} \omega dz \tag{27}$$

where $Q = 0.239$ cal/watt-sec, and ω = resistivity of cathode material. We insert

$$x^2 = a^2 - \frac{z^2}{b^2} a^2 \tag{28}$$

and integrate successively Eqs. (27) and (26) to obtain

$$T(z_1) - T(0) = \frac{I^2 \omega Q b^2}{2\pi^2 a^4 \lambda} \left(\text{arc tanh } \frac{z_1}{b} \right)^2 \tag{29}$$

12

Fig. 11. Current distribution in a spheroid.

$$T(z_1) - T(0) = \frac{I^2 \omega Q b^2}{2\pi^2 a^4 \lambda} \left[\frac{1}{2} \ln \frac{1 + (z_1/b)}{1 - (z_1/b)} \right]^2 \quad . \tag{30}$$

The first factor represents the temperature at the end of a wire of length b, radius a, heated by current I.

Now we identify x_1 with the radius of the mean emitting area $\bar{x}$ of Eq. (13) and write

$$x_1 = \bar{x} = \alpha \frac{a}{p} \tag{31}$$

where α lies between 0.25 and 0.6 as we see from Fig. 7. We apply the equation of the ellipse, inserting Eq. (31):

$$\frac{z_1}{b} = \sqrt{1 - (x_1/a)^2} = 1 - \frac{1}{2} \frac{\alpha^2}{p^2} - \frac{1}{8} \frac{\alpha^4}{p^4} \cdots \quad . \tag{32}$$

Since we assumed previously that $p \geqslant 5$ and $\alpha \leqslant 0.6$, the third term of Eq. (32) becomes negligible $(\approx 10^{-4})$.

We insert Eq. (32) into Eq. (30)

$$\varphi = \left[\frac{1}{2} \ln \frac{1 + (z_1/b)}{1 - (z_1/b)} \right]^2 \approx (\ln \frac{2p}{\alpha})^2 \quad . \tag{33}$$

The temperature rise at the tip of the spheroidal protrusion becomes

$$\Delta T = \frac{I^2 \omega Q p^2}{2\pi^2 a^2 \lambda} \cdot \varphi(p, \alpha) \tag{34}$$

where I can be found as shown previously [Eq. (13), Fig. 7], and α is a byproduct of the determination of I.

For $\alpha = 0.25 \ldots 0.6$ and $p = 5 \ldots 15$, φ has the range

$$\varphi = 5 \ldots 20 \quad . \tag{35}$$

While this report was in preparation, Tomaschke[2] published a similar analysis. Due to somewhat different simplifications his result represents essentially a fixed value of $\varphi = 8$ for $p^2 \gg 1$.
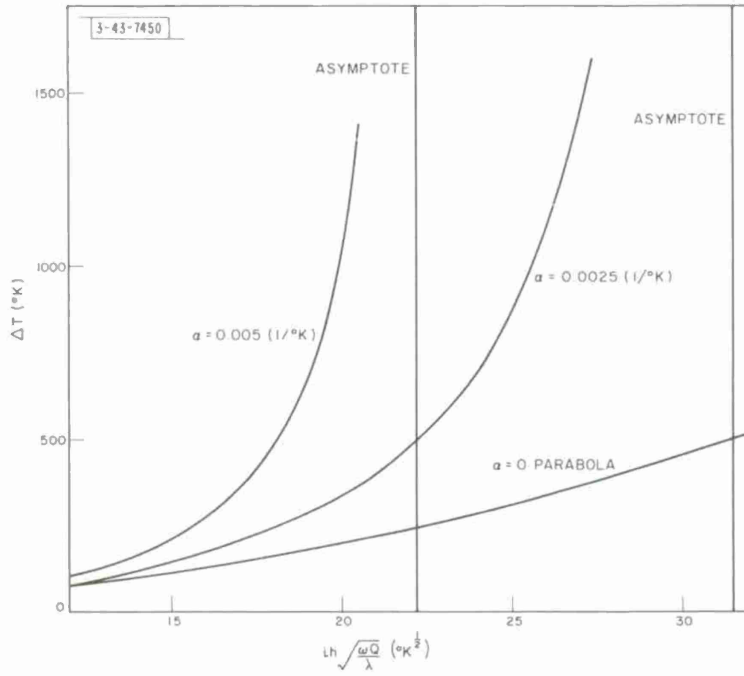
Fig. 12. Steady-state temperature of emitting whisker tip for temperature-independent resistivity and for temperature-dependent resistivity $\omega(1 + aT)$ vs normalized current density.
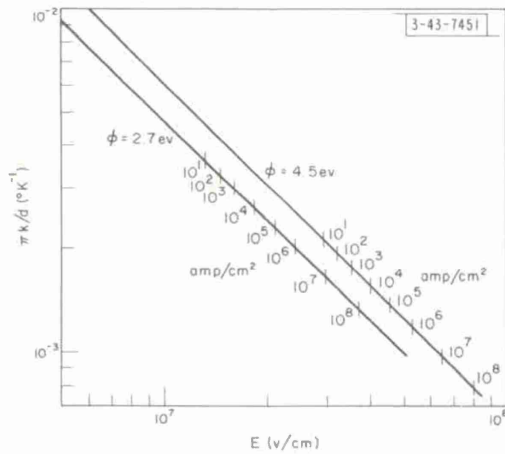

Fig. 13. Parameter $\pi k/d$ vs E for work functions of $\phi = 4.5$ and 2.7 ev.

14

B. Breakdown as Thermal Instability of the Emitting Protrusion

We consider the wire-shaped body with a rounded tip, protruding out of an infinite plane. The current density in the body is approximately equal to the emission density. The protrusions observed by Little and Whitney[19] are probably between a spheroid and a whisker. The temperature at the tip of a whisker is [for steady state, cf. Eq. (30)]

$$T - T_o = \frac{\omega Q}{2\lambda} h^2 i^2 \tag{36}$$

where ω = resistivity, $Q = 0.239$ cal/watt-sec, λ = heat conductivity, and i = current density. Ninety percent of this temperature increase is reached in the time

$$t = \frac{h^2}{k} \tag{37}$$

where k = heat diffusivity.

If the resistivity is temperature dependent, we write

$$\omega(T) = \omega(1 + \alpha T) \quad . \tag{38}$$

The appropriate solution of the heat conduction problem is given by Carslaw.[7] For steady state the temperature becomes

$$T - T_o = \frac{1}{\alpha} \left(\frac{i}{\cos ih \sqrt{\omega Q\alpha/\lambda}} - 1 \right) \quad . \tag{39}$$

From the full (time-dependent) solution we can see that 90 percent of this temperature difference is reached in the time

$$t \approx 5 \frac{h^2}{k} \tag{40}$$

for tungsten ($\alpha = 0.005$, $T - T_o = 1000°K$). According to Eq. (39), the temperature rise vs current density is plotted in Fig. 12 for $\alpha = 0.005$ and 0.0025. Most metals have values of α in this range.

The variation of current density is given for our condition by the simple relation[17]

$$i(T) = i(T = 0) \frac{\pi kT/d}{\sin \pi kT/d} \tag{41}$$

where k is Boltzmann's constant, and d is a complicated function of the field E and the work function φ.

$$\pi k/d = 2.77 \cdot 10^4 \frac{\varphi^{1/2}}{E} t(E, \varphi) \quad . \tag{42}$$

The function t is defined and tabulated on page 187 of Ref. 17. The parameter $\pi k/d$ vs E is plotted in Fig. 13 for two work functions [4.5 ev (tungsten), 2.7 ev (thoriated tungsten)]. The current densities are also noted. We see that $\pi k/d$ usually lies between 10^{-3} and $2 \cdot 10^{-3}$ as the most extreme values. It is safe, however, to consider only current densities between 10^6 and 10^8 amp/cm^2. This means that the factor $\pi k/d$ is practically a constant which is $\approx 1.5 \cdot 10^{-3}$ for thoriated tungsten and $\approx 1 \cdot 10^{-3}$ for tungsten.

If the resistivity and the current are temperature dependent, we determine the steady-state temperature by solving Eq. (39) for i:
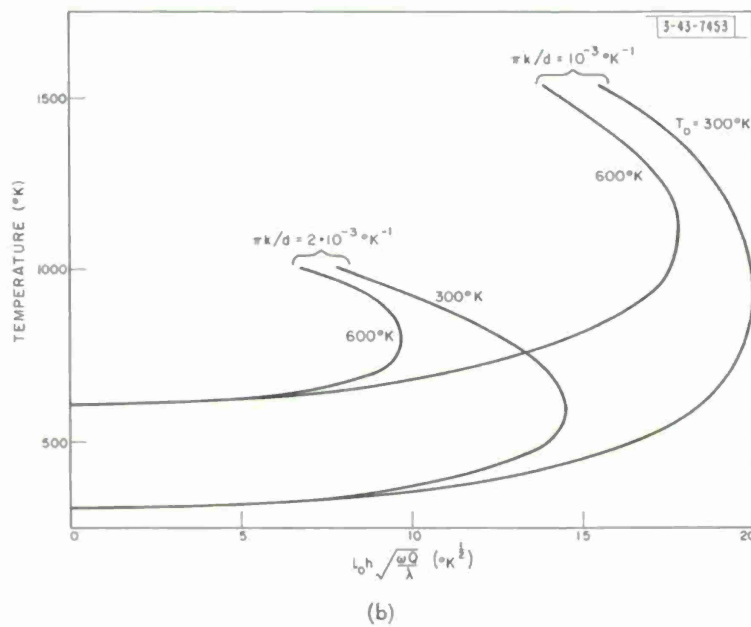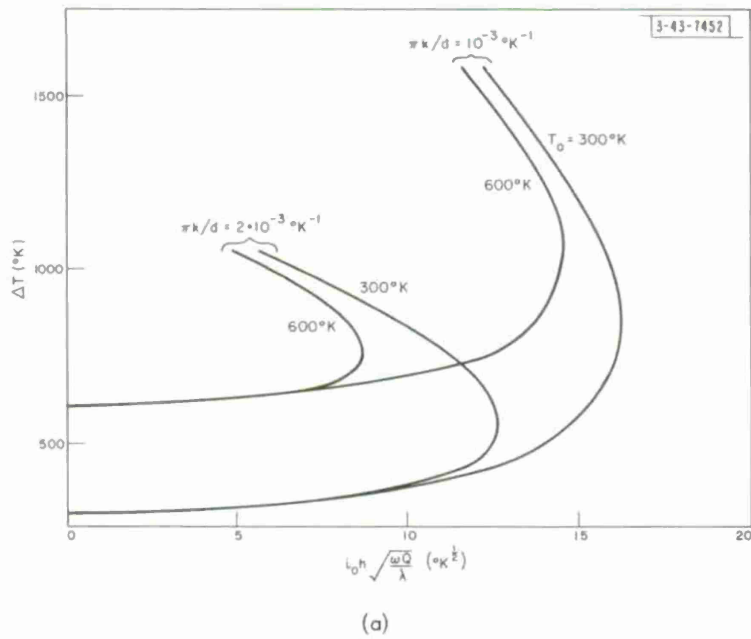
Fig. 14. Temperature at top of emitting whisker (temperature-enhanced emission) vs normalized emission of cold whisker. Temperature coefficient of resistivity: (a) $a = 0.005 \, (1/°K)$, (b) $a = 0.0025 \, (1/°K)$.

16

$$i = \frac{1}{h\sqrt{\omega Q\alpha/\lambda}} \text{ arc cos } \frac{1}{(T - T_o)\, \alpha + 1} \quad . \tag{43}$$

Inserting this into Eq. (41) we have

$$i_o = i(T = 0) = \frac{\sin \pi kT/d}{\pi kT/d} \cdot \frac{1}{h} \cdot \sqrt{\frac{\lambda}{\omega Q\alpha}} \text{ arc cos } \frac{1}{(T - T_o)\, \alpha + 1} \quad . \tag{44}$$

With this equation, we can compute the temperature T at the tip as a function of the current density of the cold protrusion, which in turn is given by the temperature-independent Fowler-Nordheim equation:

$$T(i_o) = T\, [i(E)] \quad .$$

The temperature vs this current density is plotted for several α, T_o, and $\pi k/d$ in Fig. 14. By inserting $T(i_o)$ into Eq. (44), we obtain i vs i_o as plotted in Fig. 15. These curves represent the condition of thermal equilibrium: the heat produced by the current equals the heat conducted toward the bulk of the cathode. Since we do not know the time-dependent solution of our problem, we make an estimate of the time necessary to reach equilibrium and compare Eqs. (37) and (40). In Eq. (40) the rise time is larger because we start with low energy dissipation, and only as the temperature and resistance rise, the heat production increases. This effect will be even more pronounced if the current also increases with the temperature, and we may set some limits for the rise time:

$t_1 = h^2/k \quad ,$	if T is small and the rise of resistance is negligible.
$t_2 > t_1, \text{ e.g.}, \; t_2 = 5 \cdot h^2/k \quad ,$	if T is higher and the rise of resistance is important.
$t_3 > t_2 \quad ,$	if T is still higher so that the temperature enhanced emission is also important.

We can see these three phases by comparing Fig. 14 with Fig. 12. First the temperature rises with i_o^2, then increases faster according to Eq. (39), but rather than approaching an asymptote, the curves reach an infinite slope and go into a second branch which must be unstable because the temperature and current increase while the voltage drops (i_o is a monotonic function of the applied field or voltage). If no external stabilization is used, the current must rise to infinity as soon as the infinite slope is reached and breakdown presumably occurs. The apexes of the curves in Figs. 14 and 15 thus show where breakdown occurs if the gap voltage is independent of prebreakdown current. Any larger current destroys the protrusion and causes breakdown immediately since no thermal equilibrium is possible.

C. Influence of Circuit Parameters on Instability

We consider small changes of current, etc., and the consequent changes of all other variables in the gap and in the supply network. If we specify that the emitting protrusion remains in thermal equilibrium, that is, any change follows the curves given in Figs. 14 and 15, then we can specify only one variable (i, i_o, E, or T) and all others are fixed by the equilibrium condition. Whether this equilibrium is stable or unstable can be found by comparing small changes in the
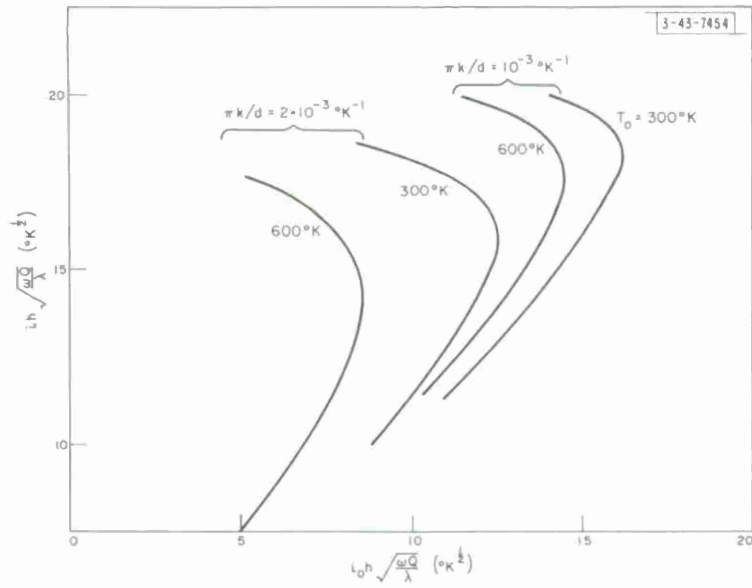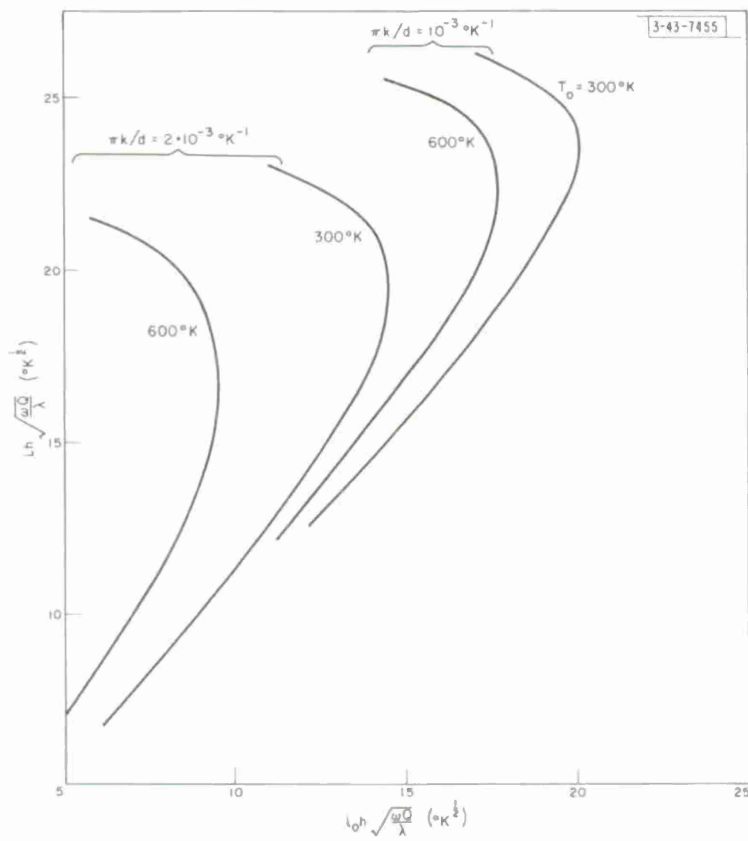
Fig. 15. Temperature enhanced emission vs cold whisker emission (both normalized). Temperature coefficient of resistivity: (a) $a = 0.005$ $(1/^\circ K)$, (b) $a = 0.0025$ $(1/^\circ K)$.

gap with the corresponding changes in the supply network. Since we have only one independent variable, we can introduce chains of any differential quotients we like, e.g.,

$$\frac{\partial E}{\partial T} = \frac{\partial E}{\partial i} \cdot \frac{\partial i}{\partial i_o} \cdot \frac{\partial i_o}{\partial T}$$

although $\partial i_o / \partial T$ may at first seem surprising since i_o is the emission at zero temperature. The partials are taken as symbols for changes in thermal equilibrium.

In an experiment, we have a resistor R in series with the spark gap and a stray capacity C parallel to it. The supply voltage is U, the gap voltage is U_G, and the gap spacing is D. The field in the gap is

$$E = \frac{U - IR}{D} \tag{45}$$

where

$$I = A \cdot i(i_o) \quad .$$

We approximate the Fowler-Nordheim equation by

$$i_o = i_{ref} \, e^{n\beta E} \tag{46}$$

$$\frac{di_o}{dE} = i_o \beta n \quad . \tag{47}$$

We now let the current increase by a small amount di. On the unstable branch of the i vs i_o curve, this implies a decrease of necessary field dE given by

$$di = \frac{\partial i}{\partial i_o} i_o \beta n dE \quad . \tag{48}$$

Because of the series resistor, the decrease of field will be

$$dE = -\frac{R}{D} \, A di \tag{49}$$

where A is the emitting area. Equation (49) inserted into Eq. (48) gives the resistance for which both changes compensate, so that the unstable curve is now an indifferent equilibrium:

$$R = -\frac{D}{n\beta A i_o \partial i / \partial i_o} \quad . \tag{50}$$

As long as $\partial i / \partial i_o$ is positive, even a negative resistance is allowed. When $\partial i / \partial i_o = \infty$, only an infinitesimal resistance is needed for stabilization.

Another important parameter is the stray capacity C. Obviously, if C is large enough, no stabilization is possible. Let us assume we have stabilized the field emission current at a certain value I by an infinite resistor and with an infinite supply voltage, in other words, by an appropriate current supply. Now let us see whether it is still stable with a stray capacity added. We assume an accidental increment of current di_A during a small time interval dt; the resulting temperature change of the emitting tip is

$$dT = \sigma di_A dt \quad . \tag{51}$$

19

The emission after dt has increased by

$$di = \frac{\partial i}{\partial i_o} \frac{\partial i_o}{\partial T} dT \quad . \tag{52}$$

This increase of emission is counteracted by a decrease of field strength and a decrease of cold emission current

$$di_o = \frac{di_o}{dE} \frac{dU_G}{D} \quad . \tag{53}$$

Since dU_G comes from the discharge of the capacity by $Adi_A dt$ coulombs,

$$di_o = \frac{di_o}{dE} \cdot \frac{Adi_A \cdot dt}{DC} \tag{54}$$

or with Eq. (47)

$$di = \frac{\partial i}{\partial i_o} \cdot \beta n i_o \cdot \frac{Adi_A \cdot dt}{DC} \quad . \tag{55}$$

Equations (52) and (51) inserted into Eq. (55) give the stationary condition, where the equilibrium is indifferent, just between stability and runaway of temperature and current. The limiting condition is thus

$$C = \frac{n\beta i_o A}{D\sigma \, \partial i_o / \partial T} \quad . \tag{56}$$

We determine σ by assuming volume heating only and neglecting any heat conduction. The temperature rise is under such conditions:

$$\frac{dT}{dt} = \frac{\omega i^2 Q}{c\rho} \tag{57}$$

or

$$\sigma = \frac{d^2 T}{dt di} = \frac{\omega Q}{c\rho} 2i \quad . \tag{58}$$

Equation (56) becomes

$$C = \frac{i_o}{i} \frac{An\beta c\rho}{2D\omega Q \, \partial i_o / \partial T} \quad . \tag{59}$$

This is the maximum allowed capacity, beyond which the upper branch in Fig. 14(a) is unstable even with an infinite resistor in series. Again the point $\partial i_o / \partial T = \infty$ is easy to stabilize since a very large capacity is allowed.

We can write Eq. (59) in another form because we can read only $d(i_o h \sqrt{\omega Q/\lambda})/dT$ from Fig. 14:

$$C = \frac{i_o n\beta c\rho \sqrt{\omega Q/\lambda}}{i2D\omega Q \, d(i_o h \sqrt{\omega Q/\lambda})/dT} \cdot hA \quad . \tag{60}$$

Since with Eq. (7),

$$A \approx \pi R^2 \approx \pi \frac{h^2}{\beta^2}$$

we see that C depends upon the third power of the size of the protrusion. This fact is a direct consequence of the volume heating from the discharge of the capacity, and it makes C very uncertain because the absolute size of the protrusion is unknown and may vary within wide limits. In any case, the first factor in Eq. (60) is roughly of the order of one, whereas h is about 10^{-4}; consequently, the stray capacity must be very small if we want to go along the unstable branch. This analysis is not yet complete because, in a spark gap, there are a number of protrusions emitting simultaneously, as many observers have reported (see Refs. 10, 11, and 19 − 22). Some authors give a Fowler-Nordheim diagram of current vs field, implying that there is only one protrusion.[23,24] Boyle, et al., explicitly state that their prebreakdown current followed the Fowler-Nordheim equation and therefore only one protrusion emits. However, Tomaschke[25] recently showed analytically that a sample of emitters with random distribution of emitting area and field intensification gives a current which follows the Fowler-Nordheim equation so closely that no experiment so far could detect the difference.

Let us look at m emitters which are still stable and rather cool ($\partial i / \partial i_o \approx 1$) and one (index e) which is reaching unstable emission. Equation (50) now becomes

$$-R = \frac{D}{\frac{\partial i_e}{\partial i_{oe}} n\beta_e A_e i_{oe} + \sum_{k=1}^{m} n\beta_k A_k i_{ok}} \qquad . \tag{61}$$

Here we have assumed that n is the same for all emitters, which is a good approximation. If we introduce the total prebreakdown current I and an average field intensification,

$$\bar{\beta} = \frac{\Sigma \, \beta_k A_k i_{ok}}{\Sigma \, A_k i_{ok}} = \frac{\Sigma \, \beta_k I_{ok}}{I - I_e} \tag{62}$$

we obtain

$$-R = \frac{D/n}{\frac{\partial i_e}{\partial i_{oe}} \beta_e I_{oe} + \bar{\beta}(I - I_e)} \qquad . \tag{63}$$

Now we let $\partial i / \partial i_{oe}$ go through infinity to negative values (unstable emission) and see that the resistance R required for stabilization is larger than that for the single protrusion because $\bar{\beta} I - \bar{\beta} I_e$ is positive and makes the denominator smaller. The necessary resistance becomes infinite for

$$-\frac{\partial i_e}{\partial i_{oe}} \beta_e I_{oe} = \bar{\beta}(I - I_e) \qquad . \tag{64}$$

Under these conditions, the unstable protrusion robs the current from those which are stable without change of external current so that the resistor does not help. But this process is limited. The current $I - I_e$ of the cold protrusions diminishes until Eq. (63) is satisfied, as long as the resistance is larger than

$$R_c = \frac{D/n}{\frac{\partial i_e}{\partial i_{eo}} \beta_e I_{oe}} \qquad . \tag{65}$$

If $R \geqslant R_c$, we should observe a jump in the current of that protrusion which becomes unstable. Breakdown may or may not occur. If R is smaller than the stabilizing resistance of the single protrusion, the protrusion should explode, after $\partial i / \partial i_o = \infty$ is reached, and breakdown should occur more easily.

We may speculate that, with a sufficiently large resistor R and other circumstances permitting, we can avoid the breakdown up to higher voltages by conditioning the gap with the prebreakdown discharge, burning away one protrusion after the other. The protrusion may be torn off as a liquid droplet or evaporate, and at the same time local heating and melting may occur at the anode. If the protrusion is destroyed without liberating too much energy, nothing may be visible since we have to expect flashes of 10^{-6} to 10^{-8} second of thermal radiation from microscopic or submicroscopic areas. Only the traces of anode material on the cathode and cathode material on the anode may be found afterward as reported by Schwabe.[11] This prebreakdown conditioning may continue until we reach either a protrusion of so low a β that too high a series resistance is required, or a protrusion of so large an area that too much prebreakdown current flows, which causes disaster somewhere else, e.g., at the anode.

VI. ELECTRON BOMBARDMENT OF THE ANODE

A. Spreading of the Electron Beam

Next we consider the spreading of the electron beam which is emitted by the protrusion. There are three causes for the spreading of the beam:

(1) Transversal initial velocity

(2) Space-charge repulsion

(3) Field distortion around the protrusion.

The initial velocity of field-emitted electrons is approximately 5 ev. The first cause is negligible.

The shape of the electron beam under acceleration and space-charge repulsion is given by Moss.[26] The equation of motion of the electrons in a circular electron beam (radius r) is

$$\frac{d^2 r}{dt^2} = \frac{e}{\epsilon_o 2\pi m} \frac{I}{\frac{e}{m} Et + \dot{z}_o} \tag{66}$$

$$z = \frac{e}{m} \frac{E}{2} t^2 + \dot{z}_o t \quad . \tag{67}$$

In our case, the initial velocity $(m/2) \dot{z}_o^2 = 5$ ev is given, and the choice of the initial condition $(dr/dt)_{t=0} = 0 \ldots 1$ does not affect the result. We take $(dr/dt)_{t=0} = 0$. Under these conditions, we can eliminate the field E as an independent parameter by introducing a new time scale $\tau = Et$ into Eqs. (66) and (67):

$$\frac{d^2 r}{d\tau^2} = \frac{e}{\epsilon_o 2\pi m} \frac{I/E^2}{\frac{e}{m} \tau + \dot{z}_o} \tag{68}$$

$$zE = \frac{e}{2m} \tau^2 + \dot{z}_o \tau \quad . \tag{69}$$

Fig. 16. Normalized current density vs normalized beam length (or anode potential) for several emission densities (space-charge effect).
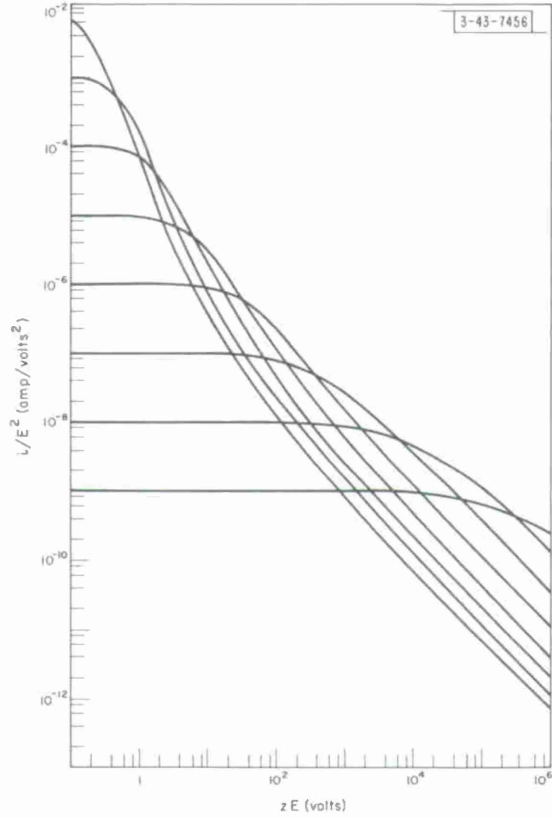
We have computed the beam shape according to a recent analysis.[8] Figure 16 shows the normalized current density vs the normalized beam length (or anode potential) for several emission densities.

In order to find the influence of the field distortion, we determine the trajectories of electrons coming from a spherical protrusion. The electrons have the following equation of motion, if we normalize the coordinates with R:

$$\frac{m}{e} \frac{d^2z}{dt^2} = \frac{\partial \Phi}{\partial z} = E_\infty \left[1 - \frac{1}{\rho^3} + 3 \frac{z^2}{\rho^5} + \frac{(\beta - 3) z}{\rho^3} \right] \tag{70}$$

$$\frac{m}{e} \frac{d^2r}{dt^2} = \frac{\partial \Phi}{\partial r} = E_\infty \left[z \frac{rz}{\rho^5} + \frac{(\beta - 3) r}{\rho^3} \right] \tag{71}$$

where

$$r = \sqrt{x^2 + y^2} \qquad \rho = \sqrt{x^2 + y^2 + z^2} \quad .$$

The above field components are found by differentiation of Eq. (3) with Eqs. (5) and (7) inserted. We see that only β remains as a parameter since we can regard $(e/m) \cdot E_\infty$ as a factor attached to the time scale which has no importance here. An example of the trajectories thus computed is given in Fig. 17. It is interesting to note that the beam radius at a large distance (e.g., $z = 10^5 R$) is less than proportional to the initial angle. This means that the current density increases toward the border of the bombarded area. This effect will partially compensate for the drop of emission density away from the center. The result of our computation is summarized in Fig. 18 as relative current density vs relative beam length for several β. This beam spreading
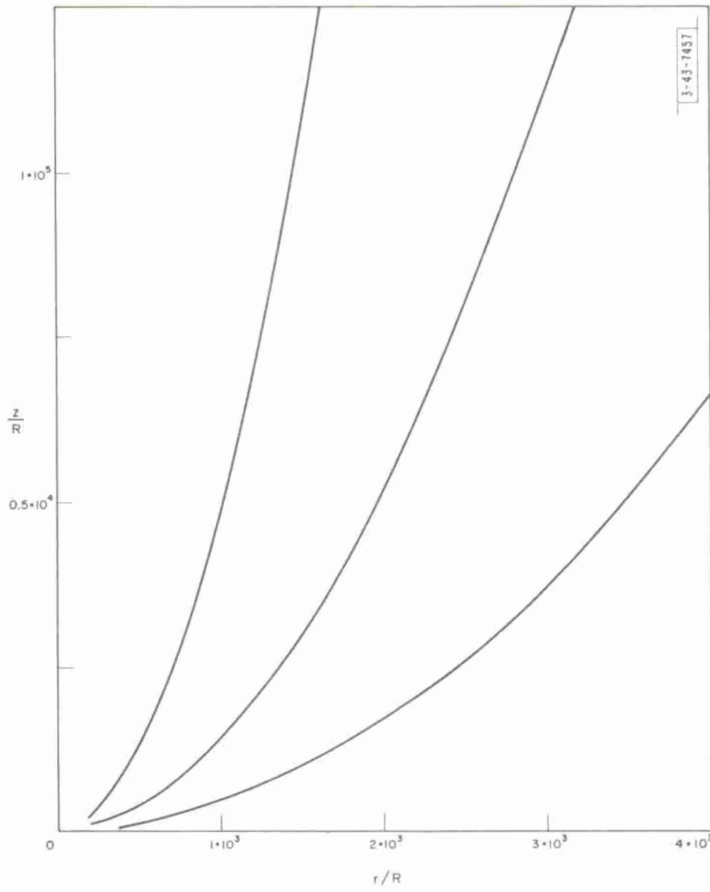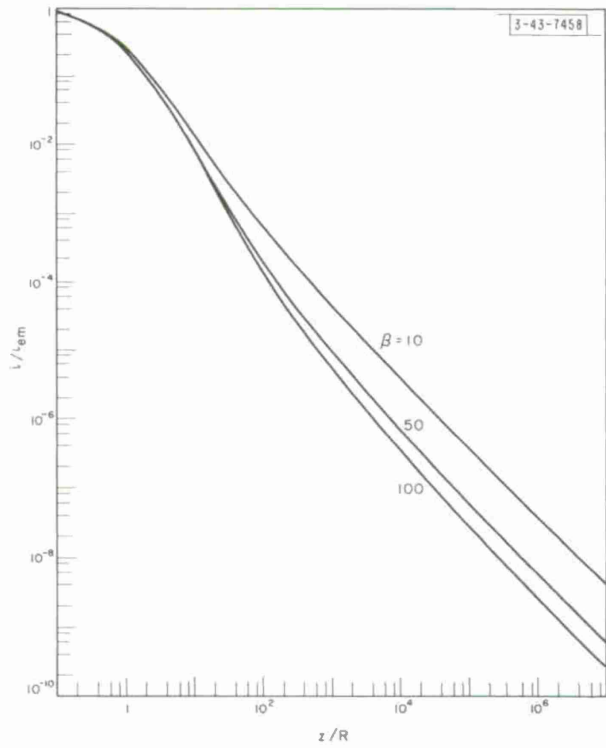
23

Fig. 17. Trajectories of electrons,
starting from a = 0, 30, and 60
degrees latitude, of the emitting
sphere.

Fig. 18. Decrease of current density due to
inhomogeneous field around emitting pro-
trusion. Space charge neglected. (Relative
current density vs relative gap length.)

24

seems to prevail slightly over the space-charge effect for most practical cases. Therefore, let us further discuss the effect of the field distortion. This field distortion is a necessary consequence of the field intensification which we need in order to have emission. The electron first moves in a radial field (radial in spherical coordinates centered at the protrusion). It acquires a radial velocity component while it is close to the protrusion. Then the parallel field takes over, and the electron approaches a parabolic trajectory. Neglecting the transition part of this motion, we approximate the radial velocity by

$$\frac{m}{2} v_r^2 = [\Phi(r = R) - \Phi(r = \infty)] e \tag{72}$$

where $\Phi(r)$ is the radial potential distribution of the protrusion,

$$\Phi(r) = \frac{q}{4\pi\epsilon_o r}$$

or with Eqs. (5) and (7),

$$\Phi(r) = \frac{E_\infty (\beta - 3) R^2}{r} \quad .$$

Now Eq. (72) becomes

$$v_r^2 = \frac{2e}{m} E_\infty (\beta - 3) R \quad . \tag{73}$$

The parabolic trajectory (oblique throw) is given by

$$-z = r tg\alpha - \frac{br^2}{2v_r^2 \cos^2\alpha} \tag{74}$$

where

$$b = \frac{E_\infty e}{m} \tag{75}$$

is the constant acceleration. Equations (73) and (75) inserted into Eq. (74) give:

$$\frac{r}{2R(\beta - 3)} = \sin\alpha \cos\alpha \pm \sqrt{\sin\alpha \cos\alpha + \cos^2\alpha \frac{z}{R(\beta - 3)}} \quad . \tag{76}$$

Since the gap width z is much greater than the radius of the protrusion, e.g., $z/R = 10^5$, we can write

$$\frac{r}{2R(\beta - 3)} = \cos\alpha \sqrt{\frac{z}{R(\beta - 3)}} \quad . \tag{77}$$

If we insert $z/R = 10^5$, $\beta = 100$ we obtain $r/R = 1.61 \cdot 10^3$ for $\alpha = 75°$, and $r/R = 6.2 \cdot 10^3$ for $\alpha = 0°$. To compare with the numerical trajectory computation, $r/R = 1.45 \cdot 10^3$ and $r/R = 5.9 \cdot 10^3$, respectively. It is understandable that our simplification gives a somewhat larger value since we overestimate the lateral displacement for three reasons:

(1) v_r is overestimated in Eq. (72) by taking $\Phi(\infty)$.

(2) v_r is assumed to exist from the start, whereas it builds up at the beginning of the trajectory.

(3) At some distance from the protrusion, the increments of v_r are no longer in the initial direction, rather they correspond to a larger α.

But we see from the example that for $\beta \geqslant 100$ the error is no more than 10 percent. The higher the β the shorter the distance over which v_r is acquired and the better our approximation. The current distribution in the beam is

$$\frac{i}{i_{em}} = \frac{R^2 d\Theta \sin \Theta}{r dr} \qquad \Theta = 90° - \alpha \quad .$$

With Eq. (77) and its derivative, we obtain

$$\frac{i}{i_{em}} = \frac{R}{4z(\beta - 3) \cos \Theta} \quad . \tag{78}$$

B. Variation of Anode Temperature vs Emitter Temperature During Conditioning

We determine how the temperature of the protrusion and the temperature of the bombarded spot at the anode change for some variations of parameters.

Case 1. Temperature of a Whisker and a Spheroid

We keep the emitting area constant, as well as β ($\beta = 100$), so that the temperature at the anode does not change. We obtain the following temperatures of the emitter.

Whisker:

$$T_1 = C_1 \frac{h_1^2}{R^4} = \frac{C_1}{h_1^2} \cdot 10^8 \tag{79}$$

with $R \approx h_1/\beta$ from Eq. (7).

Spheroid:

$$T_2 = C_1 \frac{h_2^2}{a^4} \varphi = \frac{C_1}{h_1^2} \cdot 8.5 \cdot 10^4 \quad . \tag{80}$$

Equation (80) has been obtained with $h_2 = 3h_1$, in order to compensate for the smaller emitting area of the spheroid (compare Figs. 6 and 9), and with $\varphi = 15$, and $a = h_2/15$ for $\beta = 100$ (compare Fig. 3). Index 1 refers to the whisker, and index 2 to the spheroid.

Case 2. Temperature of Different Whiskers

Emitter with Eq. (36):

$$T_{em} \sim h^2 i_o^2 \quad . \tag{81}$$

Anode with Eqs. (1) and (78) and $(\beta - 3) \approx \beta$:

$$T_a \sim U \sqrt{i_a I} \sim U \sqrt{IR i_o/\beta} \quad . \tag{82}$$

We compare a whisker before and after conditioning and assume that β has decreased while the gap voltage U has increased so that $E_\infty \beta$ remains unchanged as well as i_o. If the height h is constant, we have $R \sim 1/\beta$, $I \sim 1/\beta^2$, and $U \sim 1/\beta$:

$$\frac{T_a}{T_{em}} \sim \beta^{-3} \quad . \tag{83}$$

If the emitting area remains unchanged, we have $h \sim \beta$, and $U \sim 1/\beta$:

$$\frac{T_a}{T_{em}} \sim \beta^{-7/2} \qquad . \tag{84}$$

The real conditioning effect is, of course, not so neatly defined, but we see that the anode temperature rises quickly relative to the emitter temperature if we destroy the sharpest protrusion and decrease β accordingly (case 2), or if β remains almost constant but the persisting protrusions are less pointed (case 1).

C. Beam Spreading Compared with Anode Craters

The spreading of the electron beam by field distortion alone, as well as space charge alone, is much larger than the result given in a previous analysis by Maitland.[6] Therefore, we are going to look at the hypothesis that craters at the anode of a spark gap are due to small individual electron beams. Our argument applies with special force to small craters. The smallest spots at the anode have been observed by Hawley[27] who later with the help of an interference microscope,[28] identified them as craters. These craters have a diameter of 1.5 microns or more. They appear before breakdown, and must be due to the prebreakdown field emission.
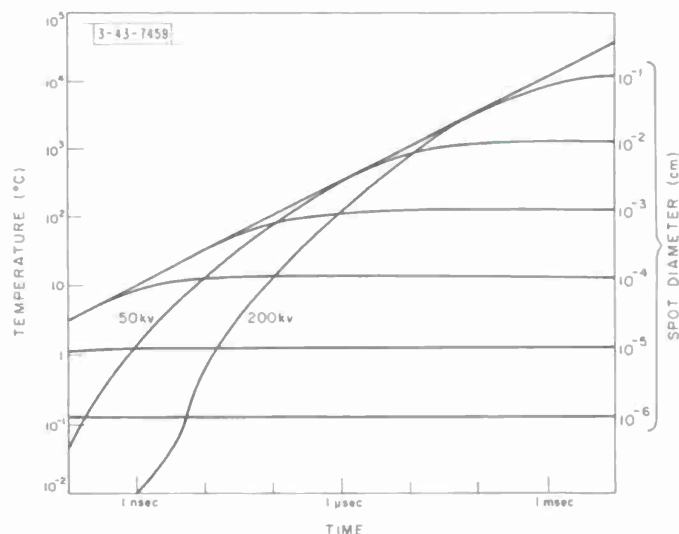

Fig. 19. Surface temperature of copper under 1-Mw/cm^2 electron bombardment.

After weak prebreakdown discharges, we have observed similar spots, sometimes around a few larger craters (e.g., 10 microns in diameter). These small spots of about a 1-micron diameter seemed to be craters, but there was lack of optical resolution. In order to melt a small circular area of copper, we need a certain power density. The temperature reached by copper under 1 Mw/cm^2 for several beam diameters is taken from Ref. 29 and shown in Fig. 19. The curves ending in horizontal lines represent surface heating of spots of different diameters; the 50- and 200-kv curves represent the heating of large diameters ($\rightarrow \infty$) with the energy dissipation vs depth taken into account. To heat a 2-micron-diameter spot to 1000°C we need about $4 \cdot 10^8$ w/cm^2. Hawley made his observations with 24 kv, 0.38-mm gap, and $6.3 \cdot 10^5$ v/cm. Thus, $4 \cdot 10^8$ w/cm^2 corresponds to a bombarding current density of

27

$$i_A = 1.7 \cdot 10^4 \, \text{amp/cm}^2 \quad .$$ (85)

We must satisfy the equations:

$$z = 3.8 \cdot 10^{-2} \, \text{cm}$$ (86)

$$r = R \sqrt{\frac{i_{em}}{i_A}} = 10^{-4} \, \text{cm} \quad .$$ (87)

We assume field distortion only and neglect the space charge. Thus, Fig. 18 gives the relationship:

$$\frac{i_{em}}{i_o} = \frac{i_{em}}{i_o} \left(\frac{z}{R} \right)$$ (88)

(β must be about 100 or more). The only solution of the simultaneous equations [Eqs. (85) through (88)] is

$$\left. \begin{array}{l} R \sim 10^{-9} \, \text{cm} \\[2ex] i_{em} \sim 1.7 \cdot 10^{14} \, \text{amp/cm} \end{array} \right\} \quad \text{for } \beta = 100 \quad .$$

Larger β gives an even more unreasonable R and i_{em}. In other words, the electron beam spreads so fast that it must come from an extremely small area with an extremely high initial current density in order to produce a single, 2-micron-diameter crater. The values of R and i are of course out of the question. This casts some doubt on the theory that each shallow crater at the anode is formed by an individual electron beam.

VII. SUMMARY

We have derived a relatively simple expression for the field intensification and emitting area of an "optimum emitter," that is, an emitter of the smallest possible height. The influence of the strong divergence of the field near the protrusion upon the field emission is computed. No observations of this effect are known to the author. An analysis of the heating of the protrusion, and of the bombarded area of the anode, shows that the thermal instability of the protrusion occurs at a much lower temperature than previously thought. Local heating of the anode is much less than previous calculations have suggested, but conditioning the cathode increases the anode heating. The computation of anode bombardment leads to an argument against the hypothesis that observed craters at the anode are produced by individual electron beams.

REFERENCES

1. R. P. Little and W. T. Whitney, "Studies of the Initiation of Electrical Breakdown in Vacuum," NRL 5944, U. S. Naval Research Laboratory (20 May 1963).

2. H. E. Tomaschke, "A Study of the Projections on Electrodes and Their Effect on Electrical Breakdown in Vacuum," Report R-192, Coordinated Science Laboratory, University of Illinois (January 1964).

3. R. Hawley, "Vacuum as an Insulator," Vacuum 10, No. 4, 310 (September 1960).

4. L. H. Bettenhausen, "High-Voltage Breakdown in Vacuum and in Oil," BMI-197-12-1, Battelle Memorial Institute (10 October 1962).

5. R. P. Little, S. T. Smith and H. D. Arnett, "Electrical Breakdown in Vacuum," NRL 5671, U. S. Naval Research Laboratory (2 October 1961), DDC 266603.

6. A. Maitland, "New Derivation of the Vacuum Breakdown Equation Relating Breakdown Voltage and Electrode Separation," J. Appl. Phys. 32, No. 11, 2399 (November 1961).

7. H. S. Carslaw and J. C. Jaeger, Conduction of Heat in Solids (Clarendon Press, Oxford, 1959).

8. G. E. Vibrans, "Computation of the Spreading of an Electron Beam Under Acceleration and Space-Charge Repulsion," Technical Report 308, Lincoln Laboratory, M. I. T. (18 April 1963), DDC 409705.

9. A. J. Ahearn, "The Effect of Temperature, Degree of Thoriation and Breakdown on Field Current from Tungsten and Thoriated Tungsten," Phys. Rev. 50, 238 (August 1936).

10. H. Tuczek, "Beitrag zur Deutung des Hochvakuumdurchschlags," Z. angew. Physik (Nukleonik) 9, No. 8, 388 (1957). (Translation No. T-154, M. D. Friedman, Inc.)

11. S. Schwabe, "Spektroskopische Bestimmung des Materialtransportes im Vordurchbruchsstadium des Hochvakuumdurchschlags," Z. angew. Physik 12, No. 6, 244 (January 1960).

12. W. P. Dyke, et al., "The Field Emission Initiated Vacuum Arc," Phys. Rev. 91, 1043 (September 1953).

13. D. Alpert and D. Lee, "Electrical Breakdown in High Vacuum," Report R-129, Coordinated Science Laboratory, University of Illinois (June 1962).

14. W. S. Boyle, P. Kisliuk and L. H. Germer, "Electrical Breakdown in High Vacuum," J. Appl. Phys. 26, No. 6, 720 (June 1955).

15. W. P. Dyke and W. W. Dolan, "Field Emission," Advances in Electronics and Electron Physics, Vol. VIII (Academic Press, New York, 1956), p. 190.

16. T. J. Lewis, "Some Factors Influencing Field Emission and the Fowler-Nordheim Law," Proc. Phys. Soc. B68, 938 (June 1955).

17. R. H. Good, Jr. and Erwin W. Müller, "Field Emission," Encyclopedia of Physics, Vol. XXI (Springer-Verlag, Berlin, 1956), p. 191.

18. T. J. Lewis, "High Field Electron Emission from Irregular Cathode Surfaces," J. Appl. Phys. 26, No. 12, 1405 (December 1955).

19. R. P. Little and W. T. Whitney, "Electron Emission Preceding Electrical Breakdown in Vacuum," J. Appl. Phys. 34, No. 8, 2430 (August 1963).

20. D. J. DeGeeter, "Photographic Observations of a Prebreakdown Discharge Transition between Metal Electrodes in Vacuum," J. Appl. Phys. 34, No. 4, 919 (April 1963).

21. M.M. Wachtel, "Field Emission from Metals at Low Applied Fields," Proceedings of the 15th Annual Conference on Physical Electronics, M.I.T. (1955).

22. H.G. Heard, "D-C Drain and Breakdown Phenomena for Unoutgassed Metals," UCRL 1697, Radiation Laboratory, University of California (March 1952).

23. W.J. Wijker, "The Electrical Breakdown in Vacuum," Appl. Sci. Res. B (Netherlands) 9, No. 1, 1 (1961).

24. E. Lyman, et al., "Vacuum Electrical Breakdown," Progress Report, Coordinated Science Laboratory, University of Illinois (June-August 1962), p. 72.

25. H.E. Tomaschke, "Field Emission from Multiple Points," Progress Report, Coordinated Science Laboratory, University of Illinois (March-May 1963), p. 81.

26. H. Moss, "A Space Charge Problem," Wireless Engineer 22, 316 (July 1945).

27. R. Hawley and C.A. Walley, "Phenomena Occurring at Electrically Stressed Metallic Surfaces in Vacuum," Nature 190, No. 4772, 252 (15 April 1961).

28. R. Hawley, "Possible Transition in the Initiating Mechanism Leading to Electrical Breakdown in Vacuum," Nature 199, No. 4897, 978 (7 September 1963).

29. G. Vibrans, "Calculation of the Surface Temperature of a Solid Under Electron Bombardment," Technical Report 268, Lincoln Laboratory, M.I.T. (16 November 1962), DDC 294645.

APPENDIX
COMPUTATION OF THE FIELD AROUND A WHISKER

We use a coordinate system $x = x'$, $z = z' + h - R$, where x' and z' are the coordinates as shown in Fig. 1. We put the sources* q_i at the points:

$$x_i = 0 \qquad z_i = \pm \frac{h - R}{n} \left(i - \frac{1}{2}\right) \qquad i = 1 \ldots n$$

$$x_i = 0 \qquad z_i = \pm(h - R) \qquad\qquad i = n + 1 \quad .$$

For the surface points, we choose the following coordinates:

$$x_j = R \qquad\qquad\qquad z_j = \frac{h - R}{n}\, j \qquad\qquad\qquad j = 1 \ldots n$$

$$x_j = R \cos\left(\frac{\pi}{2} \frac{j - n}{n}\right) \quad z_j = h - R + R \sin\left(\frac{\pi}{2} \frac{j - n}{n}\right) \quad j = n + 1 \ldots 2n \quad .$$

At the surface point j, the potential component due to source i (and its mirror image) is

$$\Phi_{ij} = H_{ij} q_i = \frac{q_i}{\sqrt{(z_j - z_i)^2 + x_j^2}} - \frac{q_i}{\sqrt{(z_j + z_i)^2 + x_j^2}} \quad .$$

The sources are determined so that the sum of the squares of the potentials becomes a minimum

$$\frac{\partial (\Phi_{ij})^2}{\partial q_i} = 0$$

$$\sum_{i>1}^{n+1} \sum_{j=1}^{2n} H_{ji} \cdot H_{jm} q_i + \sum_{j=1}^{2n} E_\infty z_j H_{jm} = 0 \quad .$$

These $n + 1$ linear equations ($m = 1 \ldots n + 1$) determine the $n + 1$ sources q_i ($i = 1 \ldots n + 1$). We check the result by computing the induced potential half way between the surface points and divide by the potential of the parallel field:

$$1 + \epsilon_p = \frac{\Phi_p}{E_\infty z_p} = \frac{1}{E_\infty z_p} \sum_{i=1}^{n+1} \left[\frac{q_i}{\sqrt{(z_p - z_i)^2 + x_p^2}} - \frac{q_i}{\sqrt{(z_p + z_i)^2 + x_p^2}} \right]$$

where

$$z_p = h - R + R \sin\left(\frac{\pi}{2} \frac{p - n - \frac{1}{2}}{n}\right)$$

$$x_p = R \cos\left(\frac{\pi}{2} \frac{p - n - \frac{1}{2}}{n}\right)$$

$$\epsilon_p = \text{relative error of approximation} \quad .$$

---

* A source q corresponds to a charge e (amp/sec) $= q/4\pi\epsilon_o$.

31

Finally we compute the induced field components $F = E_x$, $G = E_z$, and β:

$$F_{ij} = q_i x_j \, [(z_j - z_i)^2 + x_j^2]^{-3/2} - q_i x_j \, [(z_j + z_i)^2 + x_j^2]^{-3/2}$$

$$G_{ij} = q_i(z_j - z_i) \, [(z_j - z_i)^2 + x_j^2]^{-3/2} - q_i(z_j + z_i) \, [(z_j - z_i)^2 + x_j^2]^{-3/2}$$

$$F_j = \sum_{i=1}^{2n} F_{ij}$$

$$\beta = (G_{2n} + E_\infty)/E_\infty$$

$$G_j = \sum_{i=1}^{2n} G_{ij} \quad .$$

For comparison, we write also the induced components of a sphere:

$$F = \sin\left(\frac{\pi}{2} \frac{n-j}{n}\right) \left[\beta - 3 + 3\cos\left(\frac{\pi}{2} \frac{n-j}{n}\right)\right]$$
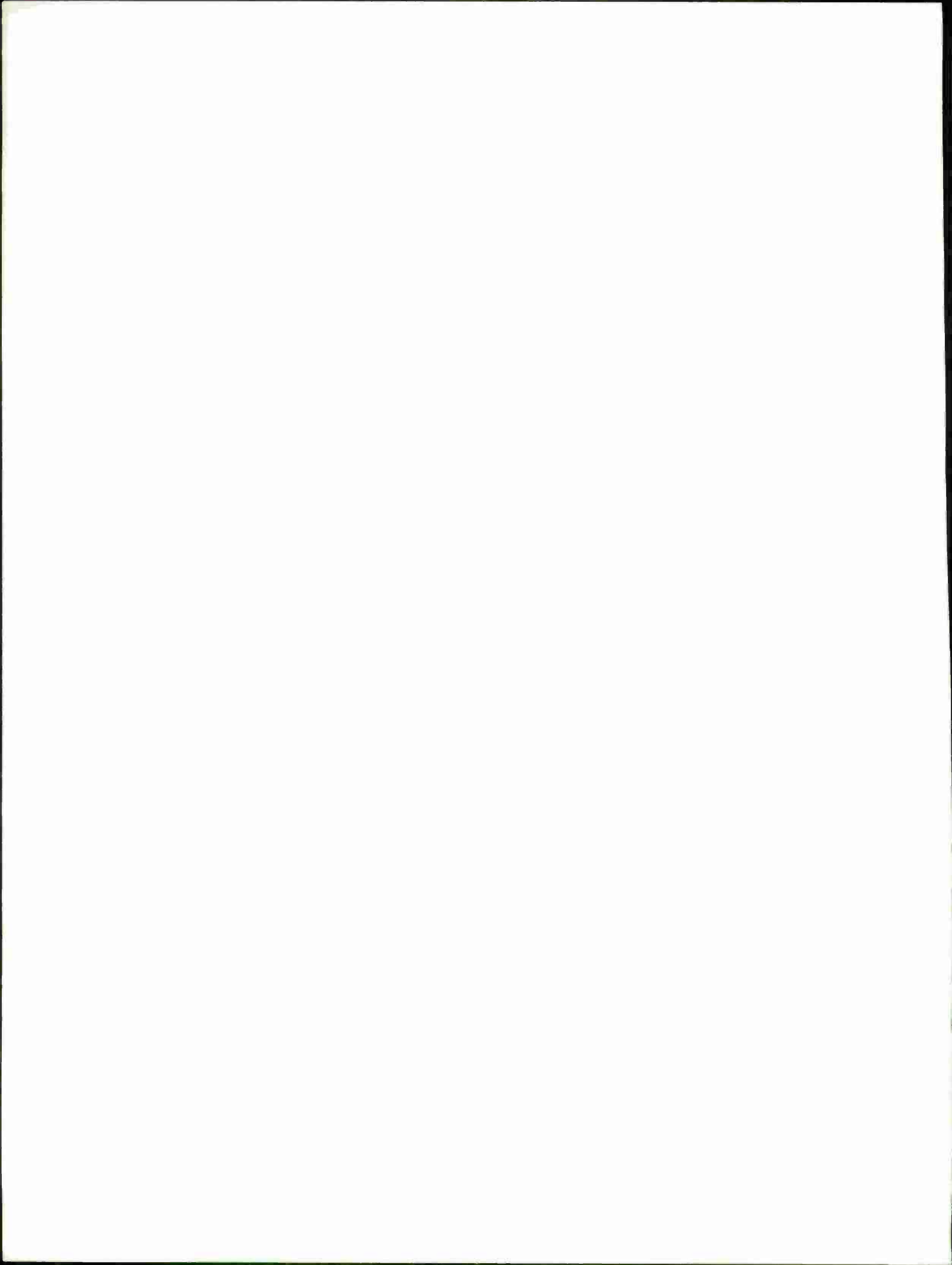
$$G = \cos\left(\frac{\pi}{2} \frac{n-j}{n}\right) \left[\beta - 3 + 3\cos\left(\frac{\pi}{2} \frac{n-j}{n}\right)\right] - 1 \quad .$$
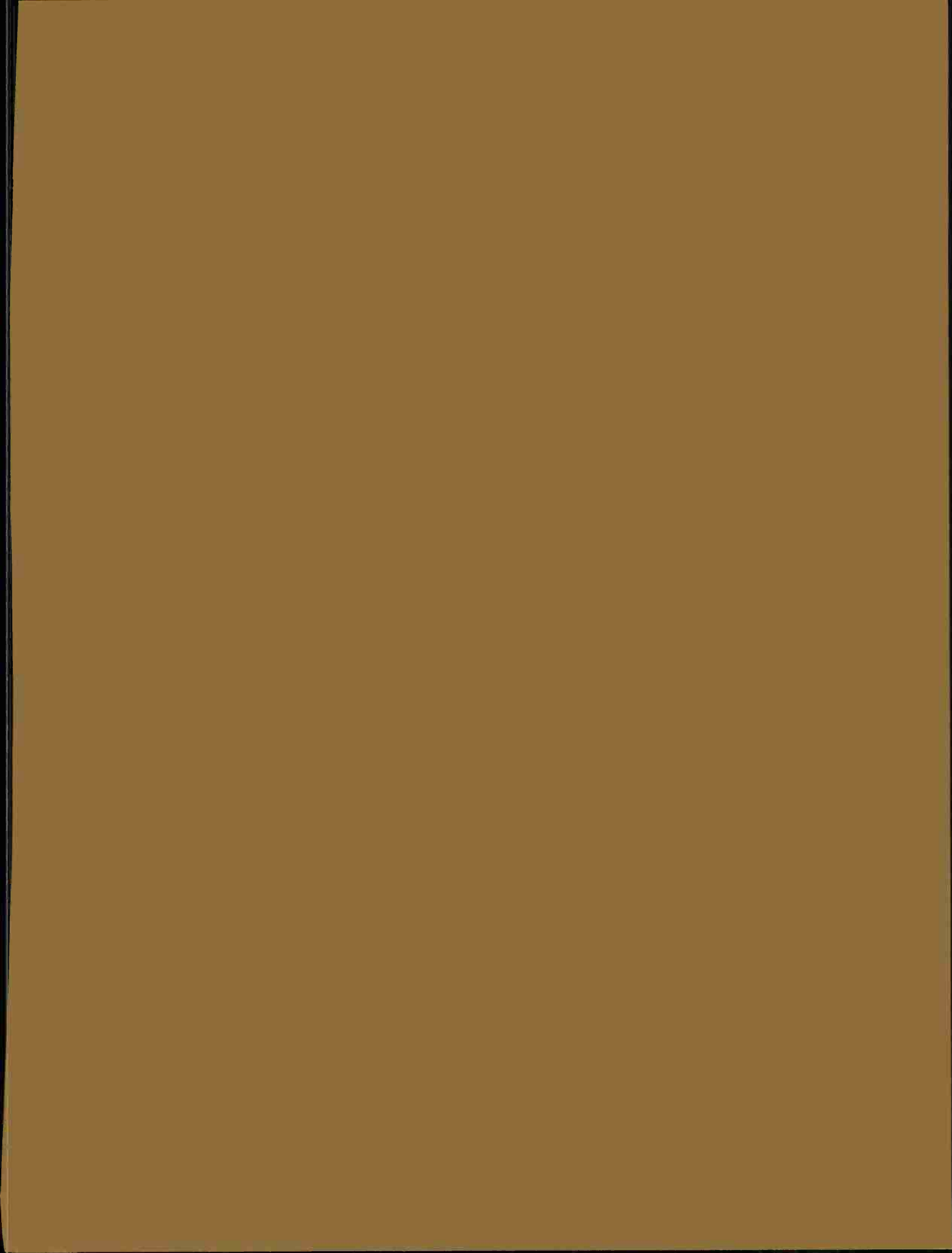
TABLE A-1					
VALUES COMPUTED FOR h = 10R, $E_\infty = -1$, AND n = 20					

$\dfrac{1+\epsilon_p}{p}$	p	$\dfrac{1+\epsilon_p}{p}$	p	q_i	i
1.262965	1	1.003059	21	−3.698786	1
0.979036	2	1.000914	22	3.610933	2
1.012559	3	0.999595	23	−3.790578	3
0.991043	4	0.998867	24	3.531658	4
1.006992	5	0.998549	25	−3.901717	5
0.994234	6	0.998504	26	3.476452	6
1.004941	7	0.998629	27	−4.040855	7
0.995678	8	0.998851	28	3.434476	8
1.003851	9	0.999116	29	−4.183174	9
0.996541	10	0.999389	30	3.370235	10
1.003140	11	0.999647	31	−4.298493	11
0.997150	12	0.999877	32	3.256939	12
1.002610	13	1.000072	33	−4.376460	13
0.997619	14	1.000232	34	3.092160	14
1.002188	15	1.000357	35	−4.448883	15
0.998044	16	1.000452	36	2.961954	16
1.001649	17	1.000520	37	−4.838017	17
0.998975	18	1.000567	38	3.872433	18
0.999647	19	1.000596	39	−8.810995	19
1.003132	20	1.000610	40	18.837837	20
				−20.341918	21

F(j)		G(j)		(j)
Whisker	Sphere	Whisker	Sphere	
−7.434622	−9.00	0.631334	1.0	20
−8.130501	−9.35272	−0.442111	−0.48042	22
−8.554745	−9.44122	−1.819855	−2.06766	24
−8.626121	−9.23262	−3.379312	−3.70423	26
−8.311287	−8.70778	−4.999279	−5.32660	28
−7.612921	−7.86400	−6.568195	−6.86400	30
−6.560654	−6.71671	−7.988472	−8.24472	32
−5.204164	−5.29944	−9.178735	−9.40078	34
−3.607761	−3.66287	−10.074983	−10.27308	36
−1.846012	−1.87138	−10.631209	−10.81582	38
−0.000000	0.0	−10.819704	−11.0	40

Whisker $\beta = 11.819704$
Sphere $\beta = 12.0$